

Quantum Monte Carlo Study of the Low-Density Two-Dimensional Homogeneous Electron Gas: Auxiliary Material

N. D. Drummond and R. J. Needs
*TCM Group, Cavendish Laboratory, University of Cambridge,
 J. J. Thomson Avenue, Cambridge CB3 0HE, United Kingdom*

TRIAL WAVE FUNCTIONS

Jastrow factors

Wigner crystals

We used the form of Jastrow factor proposed in Ref. [1]. In all our calculations we used terms of the form

$$u(r_{ij}) = \sum_l \alpha_l r_{ij}^l (r_{ij} - L_u)^3 \Theta(L_u - r_{ij}), \quad (1)$$

summed over pairs of electrons, where \mathbf{r}_{ij} is the minimum-image distance between electrons i and j , Θ is the Heaviside function, and the $\{\alpha_l\}$ and L_u are adjustable parameters (NB, L_u must be less than the Wigner-Seitz radius, and α_1 is determined by the Kato cusp conditions [2]). We also tried using terms of the form

$$\chi(r_{iI}) = \sum_m \beta_m r_{iI}^m (r_{iI} - L_\chi)^3 \Theta(L_\chi - r_{iI}), \quad (2)$$

summed over electrons i and lattice sites I , where \mathbf{r}_{iI} is the minimum-image distance between electron i and site I , and the $\{\beta_m\}$ and L_χ are adjustable parameters (NB, L_χ must be less than the Wigner-Seitz radius, and $\beta_1 = 0$ to make the wave function cusplless at the lattice sites). However, the χ term does not lower the VMC energy or variance significantly. In some of our calculations we used terms of the form

$$p(\mathbf{r}_{ij}) = \sum_S c_S \sum_{\mathbf{G} \in S} \cos(\mathbf{G} \cdot \mathbf{r}_{ij}), \quad (3)$$

summed over all pairs of electrons, where S is a symmetry-equivalent star of simulation-cell \mathbf{G} -vectors and the $\{c_S\}$ are adjustable parameters. The p term lowers the VMC energy and variance somewhat, as can be seen in Table I. The u terms in our Jastrow factors generally contained between 5 and 12 free parameters, while the p terms contained about 14 parameters.

Fermi fluids

In all our fluid calculations, both u and p terms were used in the Jastrow factor. Different parameters $\{\alpha_l\}$ were used for parallel and antiparallel spins. The addition of a p term lowers the VMC energy and variance significantly, as can be seen in Table II.

Method	p	Energy (a.u. / elec.)	Variance (a.u.)
VMC	No	-0.037 655 8(2)	0.000 080 6
VMC	Yes	-0.037 657 87(9)	0.000 078 85
DMC	No	-0.037 747 0(2)	...

TABLE I: Energy of a 64-electron, ferromagnetic, triangular Wigner crystal of density parameter $r_s = 25$ a.u. The DMC energy has been extrapolated to zero time step. A Jastrow factor containing u terms was used in all the QMC calculations; where indicated, p terms were also present. The Gaussian exponent in the crystal orbitals was $C = 0.00057$ a.u.

Method	p	BF	Energy (a.u. / elec.)	Variance (a.u.)
HF	-0.019 713 754 368	...
VMC	No	No	-0.031 623 0(4)	0.000 195 7
VMC	Yes	No	-0.031 752 39(9)	0.000 111 4
VMC	Yes	Yes	-0.031 845 3(4)	0.000 074 1
DMC	Yes	Yes	-0.031 961 9(5)	...

TABLE II: Energy of a 50-electron, paramagnetic Fermi fluid of density parameter $r_s = 30$ a.u. subject to periodic boundary conditions. The DMC energy was obtained at a single time step (4 a.u.). A Jastrow factor containing u terms was used in all the QMC calculations; p terms were also present where indicated, and electron-electron backflow (BF) functions were included where indicated.

Optimal Gaussian exponents in the crystal orbitals

In order to minimize the fixed-node error in the DMC energy, parameters that affect the nodal surface of the trial wave function may be optimized by minimizing the DMC energy. The variation of the VMC and DMC energies with the Gaussian orbital exponent for a ferromagnetic, triangular crystal of density parameter $r_s = 40$ a.u. is shown in Fig. 1. The DMC-optimized exponent is $C_{\text{DMC}} \approx 0.0003$ a.u., which is rather less than the Gaussian exponent that minimizes the VMC energy ($C_{\text{VMC}} \approx 0.0006$ a.u. with our Jastrow factor). Both are much less than the unrestricted Hartree-Fock exponent of $C_{\text{HF}} = 0.0019$ a.u. [3] The optimal exponent C_{DMC} is independent of system size, as can be seen in Fig. 1. The DMC energy of a triangular crystal at $r_s = 30$ a.u. is plotted in Fig. 2. Assuming that the DMC- and VMC-optimized exponents scale with density as $r_s^{-3/2}$ (like the

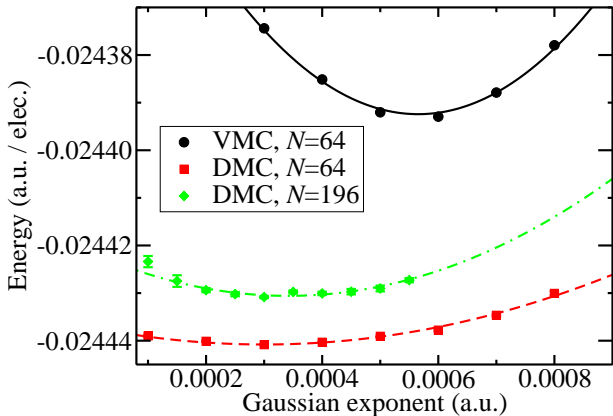


FIG. 1: VMC and DMC energies against Gaussian exponent for a 64-electron, ferromagnetic, triangular Wigner crystal of density parameter $r_s = 40$ a.u. The DMC time step was 10 a.u. and the target population was 1500 configurations for the 64-electron calculations and 512 configurations for the 196-electron calculations. The Jastrow factor was optimized for each exponent using variance minimization. The p term was used for the 196-electron calculations, but not the 64-electron ones.

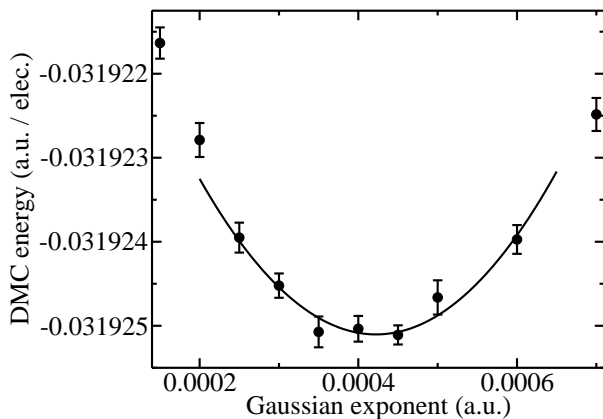


FIG. 2: DMC energy against Gaussian exponent for a 64-electron, ferromagnetic, triangular Wigner crystal of density parameter $r_s = 30$ a.u. The DMC time step was 10 a.u. and the target population was 1500 configurations. The Jastrow factor was optimized for each exponent using variance minimization. The p term was not used.

exponent within Hartree-Fock theory), we find that

$$C_{\text{VMC}} = 0.15 r_s^{-3/2} \quad (4)$$

$$C_{\text{DMC}} = 0.071 r_s^{-3/2}. \quad (5)$$

Taken together, Figs. 1 and 2 suggest that Eq. (5) is reasonable. The actual exponents used at each system size are given in Table III.

r_s (a.u.)	C (a.u.)
15	0.001 22
20	0.000 79
25	0.000 57
30	0.000 43
35	0.000 34
40	0.000 3
45	0.000 235
50	0.000 2

TABLE III: Gaussian exponents C used in our crystal calculations at each density parameter r_s .

r_s (a.u.)	DMC energy (a.u. / elec.)	
	SJ	SJB
15	-0.059 680 6(3)	-0.059 694 6(6)
20	-0.046 212 8(1)	-0.046 213 3(5)
25	-0.037 747 0(2)	-0.037 746 3(8)
30	-0.031 929 6(1)	-0.031 931 0(4)
35	-0.027 682 3(5)	-0.027 683 1(4)

TABLE IV: DMC energies of 64-electron, ferromagnetic, triangular Wigner crystals extrapolated to zero time step, with Slater-Jastrow (SJ) and Slater-Jastrow-backflow (SJB) wave functions. DMC-optimized Gaussian exponents were used in the orbitals. The target population was 1536 configurations in each case. The backflow functions were of the form described in Ref. [4], with only electron-electron terms being present.

Effect of including backflow functions

Wigner crystals

Backflow functions have only a small effect on the DMC energies of Wigner crystals, except at high densities, as can be seen in Table IV. We have not used backflow functions in any other crystal calculations.

Fermi fluids

The twist-averaged DMC energy of a 42-electron, paramagnetic Fermi fluid at $r_s = 30$ a.u., extrapolated to zero time step, is $-0.031924(2)$ a.u. per electron with a Slater-Jastrow wave function and $-0.031960(1)$ a.u. per electron with a Slater-Jastrow-backflow wave function. The backflow functions were of the form proposed in Ref. [4], with only electron-electron terms being present. We used different backflow functions for parallel- and antiparallel-spin pairs of electrons. The inclusion of backflow lowers the DMC energy by $0.000036(3)$ a.u. per electron, which is significant on the scale of the energy differences we are trying to resolve. Backflow also lowers the VMC en-

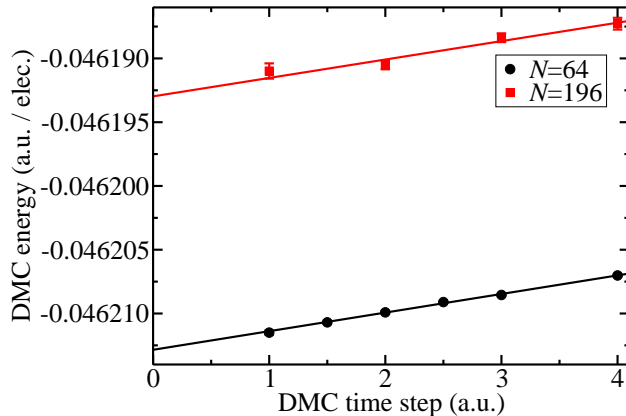


FIG. 3: DMC energy against time step for ferromagnetic, triangular Wigner crystals of density parameter $r_s = 20$ a.u. The target population was 1536 configurations and the Gaussian exponent in the orbitals was 0.00079 a.u. The Jastrow factor contained both u and p terms.

ergy and variance, as can be seen in Table II. Backflow functions were therefore used in all our fluid calculations. They contained between 5 and 12 free parameters.

SOURCES OF BIAS

Time-step bias

Wigner crystals

The finite-time-step bias in the DMC energy is linear in the time step, as can be seen in Figs. 3 and 4. The DMC energy of each crystal studied was extrapolated linearly to zero time step using at least four different time steps. The uncertainty resulting from the time-step extrapolation is included in the statistical error bars on the energy data at zero time step.

Fermi fluids

The finite-time-step bias in the DMC energy is linear in the time step, as can be seen in Fig. 5. The DMC energy of each fluid studied was extrapolated linearly to zero time step using three different time steps in each case, apart from the paramagnetic fluid at $r_s = 30$ a.u. and $N = 90$, where four time steps were used, and the paramagnetic fluids at $r_s = 35$ a.u., where two time steps were used. The uncertainty due to extrapolation is included in the statistical error bars on the energy data at zero time step.

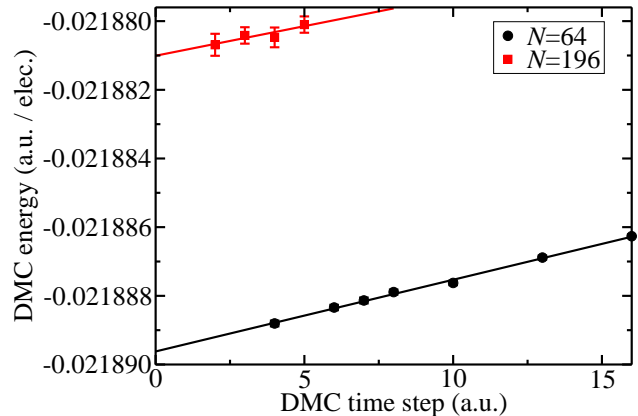


FIG. 4: DMC energy against time step for ferromagnetic, triangular Wigner crystals of density parameter $r_s = 45$ a.u. The target population was 1536 configurations and the Gaussian exponent in the orbitals was 0.000235 a.u. The Jastrow factor for the 64-electron system contained just the u term, while the Jastrow factor for the 196-electron system contained u and p terms.

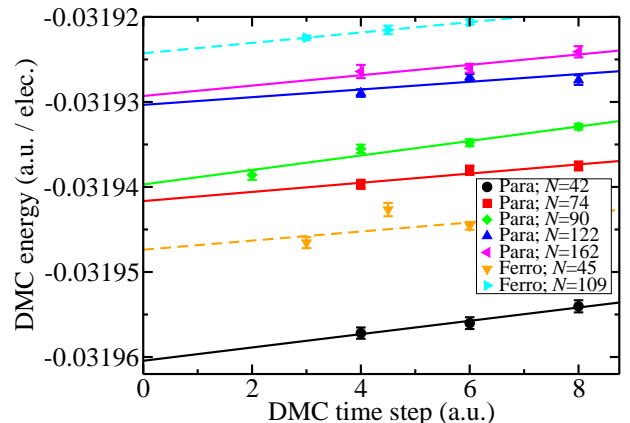


FIG. 5: Twist-averaged DMC energy against time step for Fermi fluids of density parameter $r_s = 30$ a.u. The target population was at least 1600 configurations in each case.

Population-control bias

Wigner crystals

Population-control bias is unusually severe at low density, as has previously been noticed for 3D Wigner crystals [5]. An example of population-control bias in a 2D Wigner crystal is shown in Fig. 6. The bias falls off as N_C^{-1} , where N_C is the number of configurations, as explained in Ref. [6]. At $r_s = 25$ a.u. and 64 electrons we find that the bias falls off as $0.0004/N_C$ when p terms are absent and $0.00014/N_C$ when p terms are present. We have used at least 1500 configurations in all our production runs, so that errors due to population-control bias

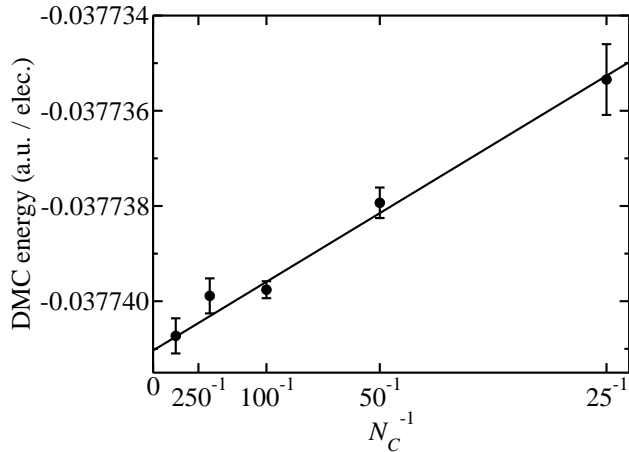


FIG. 6: DMC energy against target population for a 64-electron, ferromagnetic, triangular Wigner crystal of density parameter $r_s = 25$ a.u. The time step was 10 a.u. and the Gaussian exponent in the orbitals was $C = 0.00057$ a.u. Both u and p terms were included in the Jastrow factor.

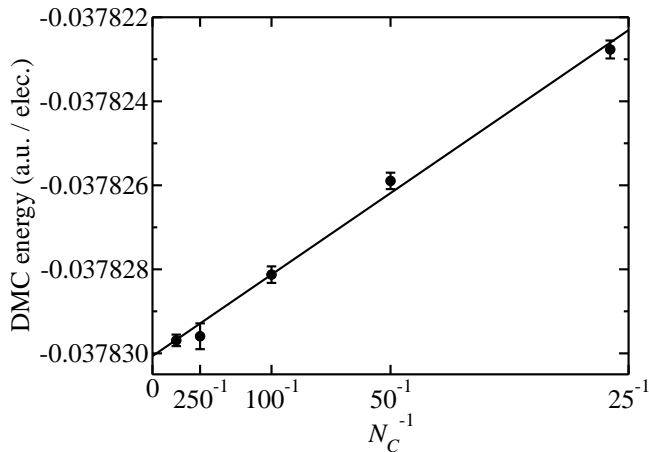


FIG. 7: DMC energy against target population for a 42-electron, paramagnetic Fermi fluid of density parameter $r_s = 25$ a.u., subject to periodic boundary conditions. The time step was 10 a.u.

are negligible.

Fermi fluids

An example of population-control bias in a 2D paramagnetic fluid is shown in Fig. 7. As with the crystal, a target population of 1500 configurations makes population-control bias negligible; we therefore used more than 1500 configurations in all our production runs.

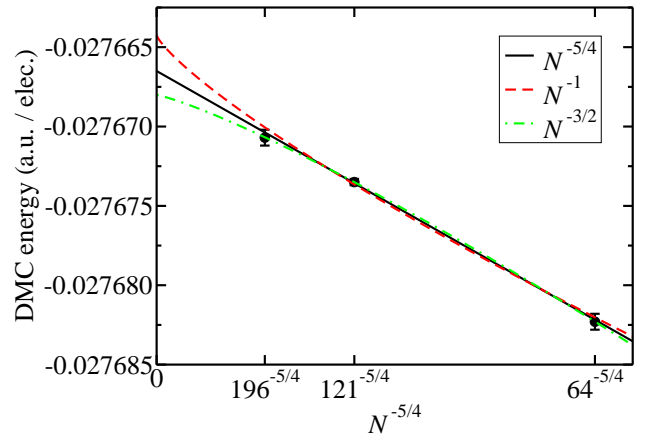


FIG. 8: DMC energy against system size N for ferromagnetic, triangular Wigner crystals of density parameter $r_s = 35$ a.u. The target population was 1536 configurations and the Gaussian exponent in the orbitals was $C = 0.00034$ a.u. The DMC energy data have been extrapolated to zero time step. We show fits of $E_N = E_\infty - bN^{-\gamma}$ for $\gamma = 5/4, 1,$ and $3/2$.

Finite-size bias

Wigner crystals

It has recently been demonstrated [7] that the finite-size errors in the energy of a 2D HEG due to (i) the neglect of long-ranged two-body correlations and (ii) the compression of the exchange-correlation hole into the simulation cell both scale as $N^{-5/4}$. Hence the energy of a 2D system should be extrapolated to infinite system size as

$$E_N = E_\infty - \frac{b}{N^{5/4}}, \quad (6)$$

where E_N is the energy per electron of the N -electron system, E_∞ is the energy per electron of the infinite system, and b is a constant. Single-particle finite-size effects are insignificant in insulators such as Wigner crystals, so we perform simulations with finite numbers of particles subject to periodic boundary conditions and extrapolate the results to infinite system size using Eq. (6). The DMC data are given in Table V, and plots of the extrapolation at $r_s = 30$ and 35 a.u. are shown in Figs. 8 and 9. In Refs. 8 and 9 it was assumed that the finite-size error scales as $N^{-3/2}$. It can be seen that the resulting extrapolation to infinite system size gives a slightly lower energy than the result we obtain by using Eq. (6).

Fermi fluids

We used square cells in all our 2D fluid calculations. Single-particle finite-size effects are very significant in

r_s (a.u.)	N	DMC energy (a.u. / elec.)
15	64	-0.059 680 6(3)
15	196	-0.059 655 9(3)
15	∞	-0.059 647 8(4)
20	64	-0.046 212 8(1)
20	196	-0.046 193 0(6)
20	∞	-0.046 186 5(8)
25	64	-0.037 747 0(2)
25	196	-0.037 731 4(4)
25	∞	-0.037 726 3(5)
30	64	-0.031 929 6(1)
30	196	-0.031 915 3(6)
30	∞	-0.031 910 6(8)
35	64	-0.027 682 3(5)
35	121	-0.027 673 5(2)
35	196	-0.027 670 7(5)
35	∞	-0.027 666 5(5)
40	64	-0.024 443 1(2)
40	121	-0.024 436 0(6)
40	196	-0.024 432 1(3)
40	∞	-0.024 428 7(4)
45	64	-0.021 889 62(7)
45	196	-0.021 881 0(5)
45	∞	-0.021 878 2(7)
50	64	-0.019 824 8(1)
50	196	-0.019 816 8(3)
50	∞	-0.019 814 2(4)

TABLE V: DMC energies of N -electron, ferromagnetic, triangular Wigner crystals of density parameter r_s , extrapolated to zero time step. Where $N = \infty$, extrapolation to infinite system size using Eq. (6) has been performed.

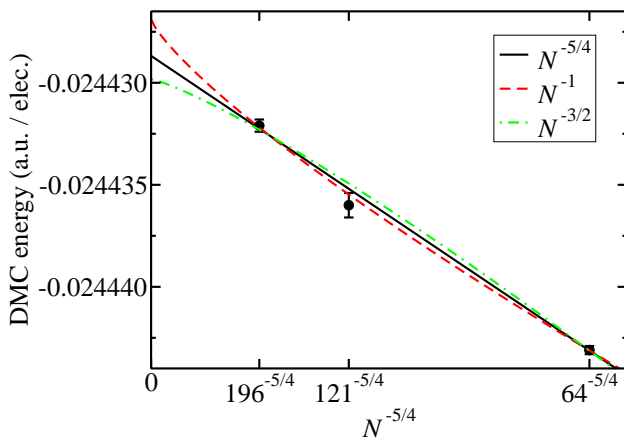


FIG. 9: DMC energy against system size N for ferromagnetic, triangular Wigner crystals of density parameter $r_s = 40$ a.u. The target population was 1536 configurations and the Gaussian exponent in the orbitals was $C = 0.0003$ a.u. The DMC energy data have been extrapolated to zero time step. We show fits of $E_N = E_\infty - bN^{-\gamma}$ for $\gamma = 5/4, 1$, and $3/2$.

r_s (a.u.)	N	DMC energy (a.u. / elec.)
20	42	-0.046 339(3)
20	90	-0.046 296(3)
20	162	-0.046 280(2)
20	∞	-0.046 267(3)
25	42	-0.037 815(1)
25	114	-0.037 782(1)
25	162	-0.037 775(1)
25	∞	-0.037 767(1)
30	42	-0.031 960(1)
30	74	-0.031 942(1)
30	90	-0.031 939 7(6)
30	122	-0.031 930(1)
30	162	-0.031 929(2)
30	∞	-0.031 923(1)
35	42	-0.027 689(1)
35	114	-0.027 670(1)
35	162	-0.027 663(1)
35	∞	-0.027 660(1)
40	42	-0.024 438(1)
40	74	-0.024 423(1)
40	114	-0.024 420(1)
40	∞	-0.024 411(2)

TABLE VI: Twist-averaged DMC energies of N -electron, paramagnetic Fermi fluids of density parameter r_s , extrapolated to zero time step. Where $N = \infty$, extrapolation to infinite system size using Eq. (6) has been performed.

Fermi fluids subject to periodic boundary conditions, because of the presence of the Fermi surface. We therefore used twist averaging within the canonical ensemble [10] to eliminate single-particle finite-size effects. The resulting DMC energies were extrapolated to infinite system size using Eq. (6). The twist-averaged DMC energies of paramagnetic, ferromagnetic, and partially polarized fluids are shown in Tables VI, VII, and VIII. An example of the extrapolation to infinite system size is shown in Fig. 10. In Refs. 8, 9, and 11 it was assumed that the bias scales as N^{-1} , which would result in an overestimate of the infinite-system energy.

The number of twist angles used ranged from a dozen or so for the larger systems that we studied to several hundred for the smaller systems. Because we sampled twist angles randomly during the simulation, the uncertainty in the energy due to the use of a finite number of twist angles is automatically included in our statistical error bars.

r_s (a.u.)	N	DMC energy (a.u. / elec.)
20	45	-0.046 284(3)
20	89	-0.046 244(1)
20	∞	-0.046 213(3)
25	45	-0.037 784(1)
25	109	-0.037 755(1)
25	∞	-0.037 740(2)
30	45	-0.031 947(1)
30	109	-0.031 924 3(6)
30	∞	-0.031 913(1)
35	45	-0.027 690 4(9)
35	89	-0.027 671 2(6)
35	∞	-0.027 657(1)
40	45	-0.024 441(1)
40	89	-0.024 426 9(6)
40	∞	-0.024 416(1)

TABLE VII: Twist-averaged DMC energies of N -electron, ferromagnetic Fermi fluids of density parameter r_s , extrapolated to zero time step. Where $N = \infty$, extrapolation to infinite system size using Eq. (6) has been performed.

N	DMC energy (a.u. / elec.)
30	-0.027 694(2)
70	-0.027 671(1)
∞	-0.027 659(2)

TABLE VIII: Twist-averaged DMC energies of N -electron Fermi fluids of density parameter $r_s = 35$ a.u. and spin polarization $\zeta = 2/5$, extrapolated to zero time step. Where $N = \infty$, extrapolation to infinite system size using Eq. (6) has been performed.

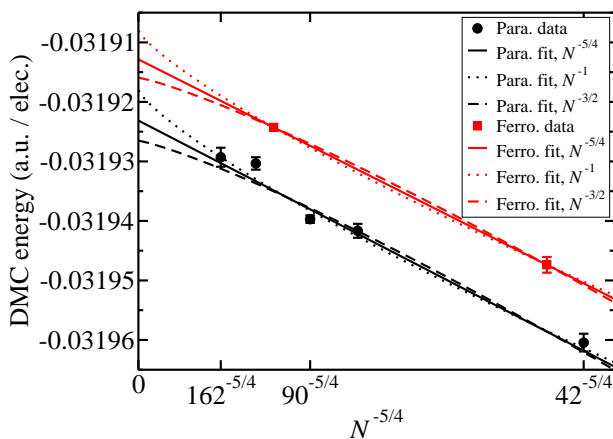


FIG. 10: Twist-averaged DMC energy against system size N for Fermi fluids of density parameter $r_s = 30$ a.u. The target population was 1600 configurations. The DMC energy data have been extrapolated to zero time step in each case. We show fits of $E_N = E_\infty - bN^{-\gamma}$ for $\gamma = 5/4, 1$, and $3/2$.

FITTING FORMULA FOR THE FLUID CORRELATION ENERGY

The Hartree–Fock energy of a 2D Fermi fluid in the thermodynamic limit is

$$E_{\text{HF}}(r_s, \zeta) = \frac{1 + \zeta^2}{2r_s^2} - \frac{2\sqrt{2}}{3\pi r_s} \left[(1 + \zeta)^{3/2} + (1 - \zeta)^{3/2} \right], \quad (7)$$

where $\zeta = (N_\uparrow - N_\downarrow)/N$ is the spin polarization. The correlation energy is defined to be $E_{\text{corr}}(r_s, \zeta) = E_{\text{fl}}(r_s, \zeta) - E_{\text{HF}}(r_s, \zeta)$, where E_{fl} is the fluid ground-state energy.

We fitted our QMC data to the parameterization of the correlation energy suggested by Rapisarda and Senatore [9]. For any particular spin-polarization ζ the correlation energy is written as

$$E_c(r_s) = a_0 \left\{ 1 + Ar_s \left[B \log \left(\frac{\sqrt{r_s} + a_1}{\sqrt{r_s}} \right) + \frac{C}{2} \log \left(\frac{r_s + 2a_2\sqrt{r_s} + a_3}{r_s} \right) + D \left(\tan^{-1} \left[\frac{\sqrt{r_s} + a_2}{\sqrt{a_3 - a_2^2}} \right] - \frac{\pi}{2} \right) \right] \right\}, \quad (8)$$

where

$$A = \frac{2(a_1 + 2a_2)}{2a_1a_2 - a_3 - a_1^2} \quad (9)$$

$$B = \frac{1}{a_1} - \frac{1}{a_1 + 2a_2} \quad (10)$$

$$C = \frac{a_1}{a_3} - \frac{2a_2}{a_3} + \frac{1}{a_1 + 2a_2} \quad (11)$$

$$D = \frac{F - a_2C}{\sqrt{a_3 - a_2^2}} \quad (12)$$

$$F = 1 + (2a_2 - a_1) \left(\frac{1}{a_1 + 2a_2} - \frac{2a_2}{a_3} \right). \quad (13)$$

The parameters a_1 , a_2 , and a_3 were determined by fitting and are given in the main text.

The fitting formula and parameter values for the crystal energy are given in the main text.

COMPARISON WITH OTHER QMC RESULTS IN THE LITERATURE

The DMC results of Rapisarda and Senatore [9] are shown in Fig. 11, along with our DMC data. The fits to fluid DMC data given by Attaccalite *et al.* [11] are also shown. Although errors due to the fixed-node approximation and population-control bias are always positive, errors due to extrapolation to infinite system size (and, to a lesser extent, extrapolation to zero time step) can be of either sign. Our DMC energies are generally lower than those of the earlier studies, due to the

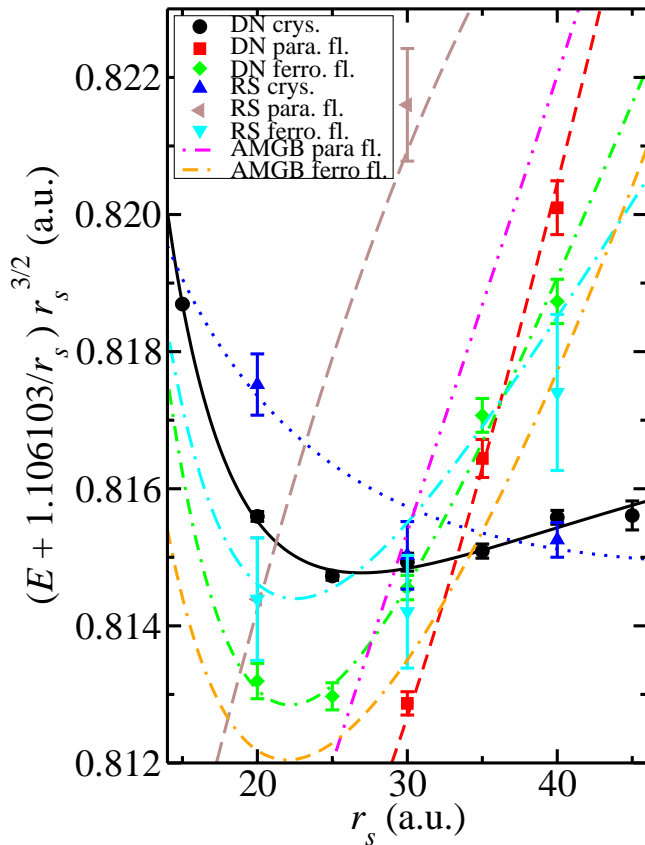


FIG. 11: DMC energy per electron E against density parameter r_s for different phases of the 2D HEG, as calculated by different authors. The Madelung energy of a triangular crystal has been subtracted from the energy and the result has been multiplied by $r_s^{3/2}$ to highlight the difference between the curves. “DN” denotes the present work, “RS” denotes the work of Rapisarda and Senatore [9], and “AMGB” denotes the work of Attaccalite *et al.* [11].

greater accuracy of the nodal surface in our calculations. Our ferromagnetic fluid energies are higher than the fit to the data of Attaccalite *et al.*, however. They corrected their Slater-Jastrow DMC data at all system sizes by adding the difference of Slater-Jastrow-backflow and Slater-Jastrow DMC energies obtained at one particular system size. It is possible that this procedure introduced non-variational errors into their data. As observed by Kwon, Ceperley, and Martin [12], the data obtained by Tanatar and Ceperley [8] are systematically too low in energy, so we have not plotted their data.

-
- [1] N. D. Drummond, M. D. Towler, and R. J. Needs, *Phys. Rev. B* **70**, 235119 (2004).
 - [2] T. Kato, *Commun. Pure Appl. Math.* **10**, 151 (1957); R. T. Pack and W. B. Brown, *J. Chem. Phys.* **45**, 556 (1966).
 - [3] J. R. Trail, M. D. Towler, and R. J. Needs, *Phys. Rev. B* **68**, 045107 (2003).
 - [4] P. López Ríos, A. Ma, N. D. Drummond, M. D. Towler, and R. J. Needs, *Phys. Rev. E* **74**, 066701 (2006).
 - [5] N. D. Drummond, Z. Radnai, J. R. Trail, M. D. Towler, and R. J. Needs, *Phys. Rev. B* **69**, 085116 (2004).
 - [6] C. J. Umrigar, M. P. Nightingale, and K. J. Runge, *J. Chem. Phys.* **99**, 2865 (1993).
 - [7] N. D. Drummond, R. J. Needs, A. Sorouri, and W. M. C. Foulkes, unpublished (2008).
 - [8] B. Tanatar and D. M. Ceperley, *Phys. Rev. B* **39**, 5005 (1989).
 - [9] F. Rapisarda and G. Senatore, *Aust. J. Phys.* **49**, 161 (1996).
 - [10] C. Lin, F. H. Zong, and D. M. Ceperley, *Phys. Rev. E* **64**, 016702 (2001).
 - [11] C. Attaccalite, S. Moroni, P. Gori-Giorgi, and G. B. Bachelet, *Phys. Rev. Lett.* **88**, 256601 (2002).
 - [12] Y. Kwon, D. M. Ceperley, and R. M. Martin, *Phys. Rev. B* **48**, 12037 (1993).